Phys Chem Minerals (2011) 38:741–752
DOI 10.1007/s00269-011-0447-y

ORIGINAL PAPER

Solid solution between lead fluorapatite and lead fluorvanadate apatite: mixing behavior, Raman feature and thermal expansivity

Qiang He · Xi Liu · Xiaomin Hu · Sicheng Li · Hejing Wang

Received: 25 March 2011 / Accepted: 24 June 2011 / Published online: 7 July 2011

Abstract The solid solution between lead fluorapatite and lead fluorvanadate apatite, $Pb_{10}[(PO_4)_{6-x}(VO_4)_x]F_2$ with x equal to 0, 1, 2, 3, 4, 5 and 6, was synthesized by solid-state reaction at 1 atm and 700°C for 72 h and characterized by scanning electronic microprobe, electronic microprobe analysis, micro-Raman spectroscopy, and powder X-ray diffraction. The volume-composition relationship at ambient temperature does not show significant deviation from the Vegard's Law. The Raman spectrum data suggest that both P and V are identical on a C_s site and both end-members show no apparent factor-group effect. The Raman frequency shift of the symmetric stretching vibration is linearly dependent on the composition. High temperature X-ray diffraction data, up to 600°C, suggest that the thermal expansion coefficients α_a, α_c, and α_V also vary linearly with the compositions of the apatites.

Keywords Lead fluorapatite · Lead fluorvanadate apatite · Raman spectrum · Solid solution · Thermal expansion

Electronic supplementary material The online version of this article (doi:10.1007/s00269-011-0447-y) contains supplementary material, which is available to authorized users.

Q. He · X. Liu (✉) · X. Hu · S. Li · H. Wang
Key Laboratory of Orogenic Belts and Crustal Evolution, MOE, Peking University, Beijing 100871, People's Republic of China
e-mail: xi.liu@pku.edu.cn

Q. He · X. Liu · X. Hu · S. Li · H. Wang
School of Earth and Space Sciences, Peking University, Beijing 100871, People's Republic of China

Introduction

Apatite is a group of minerals with geological, biological, and environmental importance (e.g., Ma et al. 1993; Lang et al. 1995; Elliott 2002). Its general formula is $M1_4M2_6(BO_4)_6X_2$, and its crystal structure is hexagonal in most cases (space group $P6_3/m$; Hughes and Rakovan 2002). In the hexagonal crystal structure, the isolated BO_4 tetrahedra ($z = 1/4, 3/4$) are linked by the M1 cations in ninefold (6 + 3) coordination and M2 cations in an irregular sevenfold (6 + 1) coordination. The triclusters of M2 cations define a large c-axis channel that accommodates the X anions. Extensive chemical substitutions can take place at all these different crystallographic sites (Pan and Fleet 2002, and references therein), with the M1 and M2 sites primarily occupied by large cations such as Na^+, Ca^{2+}, Mn^{2+}, Cd^{2+}, Ba^{2+}, Sr^{2+}, Pb^{2+}, Al^{3+}, and rare-earth elements (REE^{3+}), the B site commonly by P^{5+}, V^{5+}, As^{5+}, S^{6+}, Si^{4+}, and the X site by halides, oxy-anions, vacancies, and small neutral molecules such as H_2O. They subsequently lead to numerous solid solutions, as demonstrated by the experimental investigations of Miyake et al. (1986; $(Ca,Pb)_{10}(PO_4)_6F_2$, $(Ca,Pb)_{10}(PO_4)_6Cl_2$, and $(Ca,Pb)_{10}(PO_4)_6(OH)_2$), Kreidler and Hummel (1970; $Ca_{10}(PO_4,VO_4)_6F_2$), and Ruszala and Kostiner (1975; $Ca_{10}(PO_4)_6(Cl,OH)_2$), to name but a few. To our knowledge, however, few investigations in the literature paid much attention to the behavior of the solid solutions of apatites (e.g., Adler 1964, 1968; Baker 1966; Cockbain 1968; Kreidler and Hummel 1970; Grisafe and Hummel 1970; Boechat et al. 2000; Chernorukov et al. 2010; Knyazev et al. 2011).

Due to some environmental issues such as lead contamination of soil and high-level radioactive waste, Pb- and V-bearing apatites recently gained significant attention in the scientific world (e.g., Gupta et al. 1986; Ma et al. 1993;

Frost et al. 2003; Kim et al. 2005; Dong et al. 2005; Eon et al. 2006; Frost and Palmer 2007; Zhang et al. 2007; Liu et al. 2008, 2011a; Fleet et al. 2010; Chernorukov et al. 2010; Knyazev et al. 2011). As mentioned above, Pb and V can readily enter the structure of apatites and form compounds such as lead fluorapatite ($Pb_{10}(PO_4)_6F_2$) and lead fluorvanadate apatite ($Pb_{10}(VO_4)_6F_2$) (Merker and Wondratschek 1959). The structure of lead fluorapatite has been well determined by powder and single-crystal X-ray diffraction studies (Belokoneva et al. 1982; Suzuki et al. 1984; Miyake et al. 1986; Kim et al. 2000; Badraoui et al. 2006; Fleet et al. 2010), whereas that of lead fluorvanadate apatite is still waiting for future detailed single-crystal X-ray diffraction investigation (Merker and Wondratschek 1959). It also has been well established that there is a complete solid solution between lead fluorapatite and lead fluorvanadate apatite (Grisafe and Hummel 1970; Kreidler and Hummel 1970). Little is known about its solid solution behavior.

In the present study, we have synthesized this series of apatites and measured its Raman feature and thermal expansivity, so that its solid solution behavior can be better understood. Another study about its compressibility using diamond-anvil cell coupled with synchrotron X-ray radiation is in progress.

Experiment

A solid solution series between lead fluorapatite [$Pb_{10}(PO_4)_6F_2$] and lead fluorvanadate apatite [$Pb_{10}(VO_4)_6F_2$], with its composition of $Pb_{10}[(PO_4)_{6-x}(VO_4)_x]F_2$ (x designed as 0, 1, 2, 3, 4, 5 and 6; Table 1), was synthesized in a conventional muffle furnace via solid-state reaction. The starting materials used in the synthesizing experiments were mechanical powder mixtures made of lead fluoride (PbF_2), lead oxide (PbO), phosphorus pentoxide (P_2O_5), and vanadium oxide (V_2O_5). Since P_2O_5 powder readily absorbs moisture from air, we added to the starting materials 5% more P_2O_5 than required by the chemical formulas (by weight). These mixtures were pretreated at 110°C in a drying oven for 48 h and then encapsulated in Pt tubes with a diameter of 5 mm and a length of 50 mm by using arc-welding technique. The synthesizing conditions were 1 atm, 700°C, and 72 h. According to the literature data (e.g., Grisafe and Hummel 1970; Kreidler and Hummel 1970; Podsiadlo 1990; Zhang et al. 2007; Liu et al. 2008, 2011a; Chernorukov et al. 2010; Knyazev et al. 2011), synthesizing apatites with the solid-state reaction method is generally easy, and apparent apatite formation has been demonstrated down to at least 300°C in a few hours. For the lead apatites, the melting point of $Pb_{10}(PO_4)_6F_2$ at 1 atm is about 1,098°C (Podsiadlo 1990), whereas that of $Pb_{10}(VO_4)_6F_2$ has not been experimentally determined yet. Since the complete replacement of PO_4 by VO_4 lowers the melting temperature by about 150°C in the solid solution of $Pb_{10}(PO_4)_6Cl_2$–$Pb_{10}(VO_4)_6Cl_2$ (Chernorukov et al. 2010), the melting temperature of $Pb_{10}(VO_4)_6F_2$ is most likely close to about 900°C. Our synthesizing temperature of 700°C, therefore, should not be far away from the melting curve of the solid solution of $Pb_{10}[(PO_4)_{6-x}(VO_4)_x]F_2$, which in turn should promote the equilibrium state in the synthesizing experiments.

We examined the synthetic products by using optical microscopy, scanning electron microscopy (SEM; Quanta 200 FEG), powder X-ray diffraction (XRD; X'Pert Pro MPD system), and electron microprobe analysis (EMPA; JEOL JXA-8100). The EMPA analytical conditions were as follows: accelerating voltage 15 keV, beam current 10 nA, 30 s counting at peak, and 10 s on background. The instrument was calibrated for Pb, V, and P using standards of $PbCrO_4$-crocoite (Tasmania, Australia; SPI standard #20), synthetic V–P–K–O glass (SAC/TC38), and $Ca_{10}(PO_4)_6F_2$-apatite (Ontario, Canada; SPI standard #4), respectively. We applied the ZAF correction procedure to all EMPA analyses. The F content was not analyzed by the electron microprobe in the wavelength dispersive mode, but examined by it in the energy dispersive mode.

Raman spectra were collected on polished single crystals of the apatites with a confocal micro-Raman system (Renishaw system RM-1000) in a back-scattering geometry at ambient temperature (25°C). All samples were excited by the 514.5 nm line of an Ar^+ ion laser operating at 20 mW. The Raman spectra were recorded with a counting time of 10 s, a data range from 200 to 2,000 cm^{-1}, 1 accumulation, a slit of 50 μm, and a 20× objective. The corresponding spectral resolution was 1 cm^{-1}.

High-T X-ray diffraction data were collected by using an X'Pert Pro MPD system, which had an attached Anton Paar HTK-1200 N oven running with a Eurotherm temperature controller (Eurotherm 2604; type S thermocouple checked against the melting point of NaCl). This heating system can reach 1,200°C with an accuracy of ±2°C. Other details of the X'Pert Pro MPD diffractometer system include a Cu target, operation voltage of 40 kV, and current of 40 mA, as used in our previous studies (Liu et al. 2010, 2011b; Hu et al. 2011). High-T experiments were conducted up to 800°C, and the heating and data-collection procedures were as follows: after collection of the X-ray diffraction data at a given temperature, the sample was heated up to the next setpoint by 10°C/min and then allowed to relax for 5 min before collection of the powder diffraction spectrum. X-ray data were collected between 10 and 70°2θ, with a scanning step length of 0.017°2θ and a scanning time of 10 s for each scanning step. The alignment of the X-ray diffractometer system was done with a standard of silicon crystalline powder at ambient temperature only. Due to the

Table 1 Composition of apatite solid solution $Pb_{10}[(PO_4)_{6-x}(VO_4)_x]F_2$

Sample #	Targeted x	Apatite (wt%)[a]			Pb/(P + V) (mol%)[b]	Trace phase[c] (wt%)	
		Pb	P	V		Pb	V
HL019	0	77.2 (6)[d]	7.4 (2)	–	1.56 (1)	–	–
HL020	1	76.2 (8)	6.9 (1)	1.0 (1)	1.52 (2)	91.4 (17)	–
HL021	2	77.2 (8)	5.6 (2)	2.7 (3)	1.60 (5)	25.0 (4)	41.7 (5)
HL016	3	76.6 (6)	3.5 (2)	6.3 (2)	1.56 (3)	84.3 (6)	4.5 (2)
HL017	4	76.6 (4)	2.7 (3)	7.8 (3)	1.54 (4)	24.2 (8)	42.2 (2)
HL018	5	76.4 (8)	0.8 (1)	10.4 (2)	1.61 (3)	84.7 (10)	4.9 (4)
HL010	6	75.3 (7)	–	12.3 (1)	1.51 (2)	–	–

[a] Composition of apatites analyzed by EMPA

[b] Calculated from the EMPA data, suggesting either Pb underestimated, or (P + V) overestimated, or these apatites non-stoichiometric (the ideal Pb/(P + V) ratio of apatites is 1.67)

[c] The trace phase appears as melt in HL016 and HL018, whereas it appears as solid phase in HL020, HL021, and HL017 (Fig. 1). No P is apparently detected for the trace phase in all samples

[d] Number in the parentheses represents one standard deviation in the rightmost digit; for each sample, more than 10 EMPA analyses were made on the apatite, whereas 5 EMPA analyses were typically made on the trace phase

thermal expansion of the furnace and sample holder components and the powder sample itself, the sample position was slightly changed at high temperatures. Following the data-processing procedure verified in Hu et al. (2011), the influence of this small sample displacement was appropriately corrected by a full powder X-ray pattern refinement using the MDI's program Jade 5.0 (Material Data, Inc.), which led to unit-cell parameters with high accuracy.

Results and discussion

The electron back-scatter images (Fig. 1) showed that the synthesizing experiments with the intermediate starting compositions produced two phases, with the dominant phase identified as apatite by the powder X-ray diffraction data (Fig. 2). The trace phase, varying from experiment to experiment (Table 1), attained a volume proportion up to at most 5%, so that it could not be readily detected by the X-ray. Here, we want to point out that the presence of some trace phase in the apatite-synthesizing experiments using solid-state reaction method seems very common (Zhang et al. 2007; Liu et al. 2011a), although in most investigations, no critical SEM examination was conducted to check for it (Grisafe and Hummel 1970; Kreidler and Hummel 1970; Chernorukov et al. 2010; Knyazev et al. 2011). Since the main subject of this study is about the solid solution behavior of lead fluorapatite and lead fluorvanadate apatite, it is appropriate to ignore the trace phases.

The EMPA data (Table 1) suggested that the compositions of the lead apatites $Pb_{10}[(PO_4)_{6-x}(VO_4)_x]F_2$ were generally homogeneous, indicating good equilibrium state in our synthesizing experiments. Considering the high synthesizing temperature and the long experimental duration, this is not surprising. On the other hand, the EMPA data potentially suggested that these synthetic lead apatites might be non-stoichiometric: the Pb/(P + V) molar ratio of the lead apatites (1.56 ± 0.04) ranges from 1.51 to 1.60. Previously, Liu et al. (2008) and Fleet et al. (2010) observed a non-stoichiometry for their synthetic lead apatites prepared by using the solid-state reaction method (Pb/(P + V) = 1.56). In comparison, Boechat et al. (2000) observed a non-stoichiometry for their synthetic calcium phosphate and vanadate apatite solid solution prepared by precipitation from solutions (the Ca/(P + V) ratio, from 1.72 to 1.83, is much larger than the ideal value of 1.67). It thus appears that synthetic apatites are usually non-stoichiometric, which is apparently incompatible with the well-known fact of ready and extensive substitution of different ions in the apatite structure. Further examination of the EMPA data from this study suggests (Table 1 and SIFig. 1 of the Supplementary Information), however, that the measured Pb contents of the apatites are not accurate enough, but the measured P and V contents are generally overestimated (the overestimation is about 15% in the case of P while it is about 20% in the case of V). It follows that the non-stoichiometry of synthetic apatites might be just an artifact caused by the EMPA analytical method; apatites are infamous for quantitative analyses because of the combination of F (Cl or OH) and O, and good standards for Pb and V are usually unavailable. We therefore tend to believe that our synthetic lead apatite solid solution $Pb_{10}[(PO_4)_{6-x}(VO_4)_x]F_2$ compositionally met our original designs.

Mixing behavior

Powder X-ray diffraction patterns at ambient *P–T* conditions, shown in Fig. 2, clearly indicate that the major

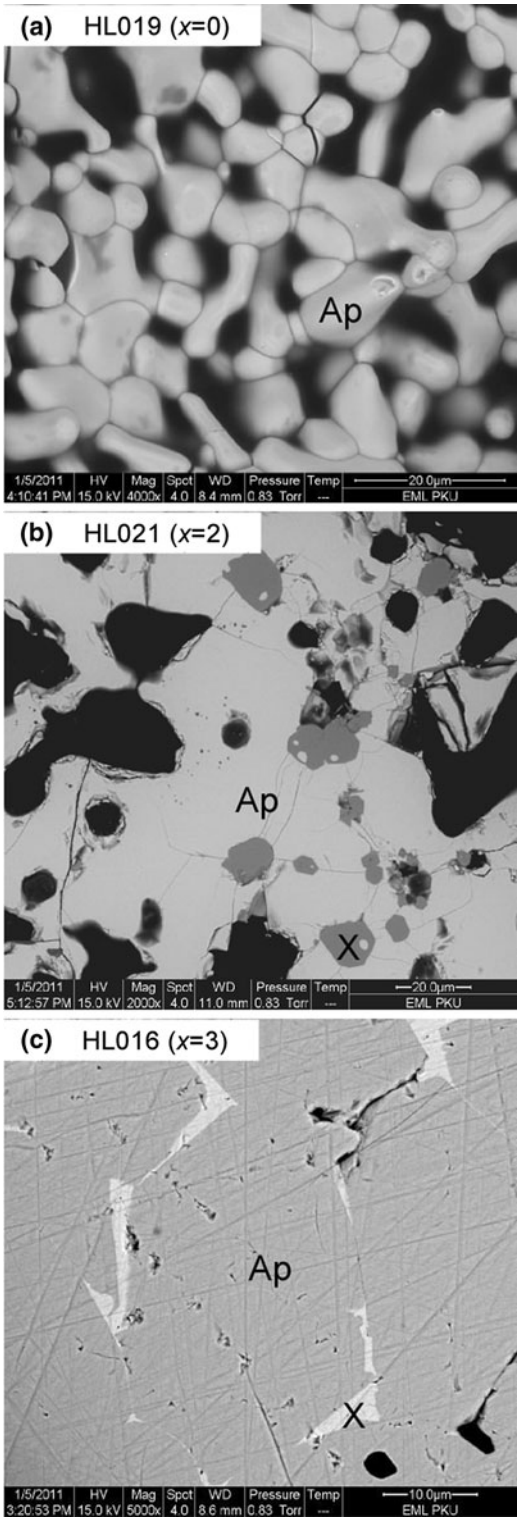

Fig. 1 Electron back-scatter images showing the textures of the synthesized materials: **a** HL019, **b** HL021, and **c** HL016. *Ap* apatite, *X* unidentified trace phase. The unidentified trace phase appears as a V_2O_5-rich crystalline phase in HL021, whereas it appears as a PbO-rich melt-like phase in HL016. To better illustrate the textures, we deliberately selected to show here the trace phase-enriched parts of the experimental products

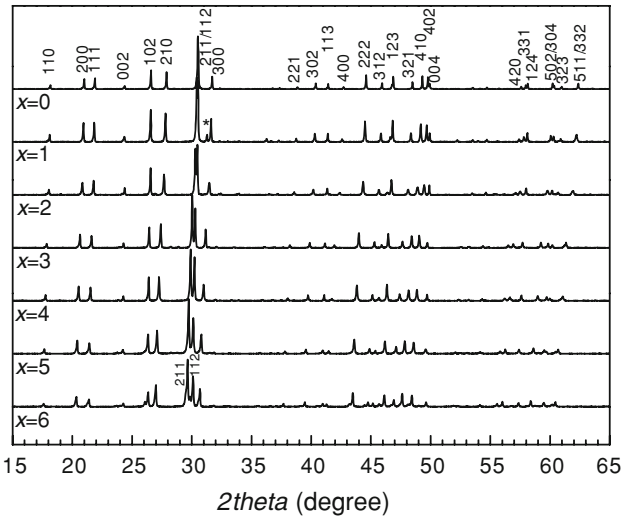

Fig. 2 XRD patterns of the apatite solid solution $Pb_{10}[(PO_4)_{6-x}(VO_4)_x]F_2$ at room temperature. All major peaks but one (indicated by the *asterisk*) can be assigned to apatite. For the two samples with $x = 5$ and $x = 6$, slight peak-splitting was observed but not obvious in this diagram (see Supplementary Information for more detailed illustration)

products from the synthesizing experiments are indeed apatites. For the two samples with high vanadium content ($x = 5$ and 6), some splitting of the diffraction peaks was observed (see more details in SIFig. 2 of the Supplementary Information), potentially suggesting slight crystal structure distortion. Similar phenomenon was observed for the calcium fluorarsenate and fluorvanadate apatites with more than 80% P replaced by V (Grisafe and Hummel 1970; Mercier et al. 2007).

The unit-cell parameters of $Pb_{10}(PO_4)_6F_2$ (Table 2) are much comparable to the values given out by Merker and Wondratschek (1959), Kreidler and Hummel (1970), Grisafe and Hummel (1970), Kim et al. (2000), Liu et al. (2008) and Fleet et al. (2010), but in disagreement with Knyazev et al. (2011). Presumably, the apatites synthesized by Knyazev et al. (2011) were of the composition $Pb_9(PO_4)_6$, considering the close agreement of the unit-cell parameters from the studies of Knyazev et al. (2011) and Hata et al. (1980; more discussion later). In addition, the unit-cell parameters of $Pb_{10}(VO_4)_6F_2$ (Table 2) are also much comparable to the values given out by Merker and Wondratschek (1959), Kreidler and Hummel (1970), and Grisafe and Hummel (1970).

The unit-cell parameters of the solid solution of the lead apatites $Pb_{10}[(PO_4)_{6-x}(VO_4)_x]F_2$ at ambient *P–T* conditions are shown in Fig. 3. For this solid solution, the replacement of P by V causes the *a*-axis of the apatites to expand (up to about 3.4%), but leaves the *c*-axis more or less unchanged (less than 1%), leading to a decreased *c*/*a* ratio of the unit cell (up to about 2.7%). Obvious in Fig. 3 is the

Table 2 Unit-cell parameters of apatite solid solution $Pb_{10}[(PO_4)_{6-x}(VO_4)_x]F_2$

T (°C)	a (Å)	c (Å)	V (Å^3)	c/a
$x = 0$				
26	9.7757 (2)[a]	7.3046 (1)	604.54 (3)	0.74722 (2)
100	9.7905 (2)	7.3139 (1)	607.14 (3)	0.74704 (2)
200	9.8120 (2)	7.3314 (2)	611.27 (3)	0.74719 (2)
300	9.8342 (2)	7.3512 (2)	615.70 (4)	0.74751 (2)
400	9.8565 (2)	7.3715 (2)	620.21 (5)	0.74788 (3)
500	9.8786 (2)	7.3945 (2)	624.93 (4)	0.74854 (3)
600	9.9026 (2)	7.4226 (3)	630.36 (4)	0.74956 (3)
$x = 1$				
26	9.7976 (5)	7.3016 (3)	607.00 (6)	0.74525 (5)
100	9.8129 (3)	7.3126 (2)	609.81 (4)	0.74520 (3)
200	9.8358 (5)	7.3319 (3)	614.29 (7)	0.74543 (5)
300	9.8589 (3)	7.3530 (2)	618.95 (5)	0.74583 (3)
400	9.8820 (3)	7.3751 (2)	623.73 (5)	0.74632 (3)
500	9.9056 (3)	7.3983 (3)	628.67 (5)	0.74688 (4)
600	9.9282 (5)	7.4232 (5)	633.67 (7)	0.74768 (6)
$x = 2$				
26	9.8544 (5)	7.3104 (3)	614.79 (7)	0.74184 (5)
100	9.8711 (5)	7.3229 (2)	617.94 (6)	0.74185 (4)
200	9.8942 (5)	7.3428 (3)	622.52 (7)	0.74213 (5)
300	9.9180 (4)	7.3641 (1)	627.33 (5)	0.74250 (3)
400	9.9436 (6)	7.3891 (3)	632.71 (8)	0.74310 (5)
500	9.9651 (6)	7.4098 (3)	637.24 (8)	0.74357 (5)
600	9.9891 (11)	7.4334 (6)	642.34 (15)	0.74415 (10)
$x = 3$				
26	9.9466 (3)	7.3324 (2)	628.25 (4)	0.73718 (3)
100	9.9641 (3)	7.3459 (2)	631.62 (4)	0.73723 (3)
200	9.9881 (3)	7.3668 (2)	636.46 (4)	0.73756 (3)
300	10.0113 (3)	7.3879 (2)	641.26 (4)	0.73795 (3)
400	10.0361 (4)	7.4102 (3)	646.39 (5)	0.73835 (4)
500	10.0594 (3)	7.4339 (2)	651.46 (5)	0.73899 (3)
600	10.0842 (4)	7.4620 (3)	657.16 (6)	0.73997 (4)
$x = 4$				
26	9.9925 (2)	7.3328 (1)	634.09 (3)	0.73383 (2)
100	10.0100 (2)	7.3465 (1)	637.49 (3)	0.73392 (2)
200	10.0349 (3)	7.3678 (2)	642.53 (4)	0.73422 (3)
300	10.0597 (3)	7.3913 (2)	647.77 (4)	0.73474 (3)
400	10.0863 (3)	7.4177 (2)	653.53 (4)	0.73543 (2)
500	10.1098 (2)	7.4416 (1)	658.69 (3)	0.73608 (2)
600	10.1339 (4)	7.4692 (3)	664.29 (5)	0.73706 (4)
$x = 5$				
26	10.0625 (4)	7.3525 (3)	644.73 (6)	0.73068 (5)
100	10.0808 (4)	7.3675 (4)	648.39 (6)	0.73084 (5)
200	10.1101 (2)	7.3996 (2)	655.01 (4)	0.73191 (3)
300	10.1338 (2)	7.4197 (2)	659.87 (3)	0.73218 (2)
400	10.1555 (2)	7.4415 (2)	664.64 (3)	0.73276 (2)
500	10.1775 (3)	7.4661 (2)	669.74 (4)	0.73359 (3)
600	10.2004 (3)	7.4961 (2)	675.46 (4)	0.73488 (3)

Table 2 continued

T (°C)	a (Å)	c (Å)	V (Å^3)	c/a
$x = 6$				
26	10.1101 (5)	7.3529 (3)	650.89 (13)	0.72728 (5)
100	10.1307 (4)	7.3726 (3)	655.28 (11)	0.72775 (4)
200	10.1605 (2)	7.4059 (2)	662.12 (6)	0.72889 (3)
300	10.1844 (2)	7.4282 (2)	667.24 (6)	0.72937 (2)
400	10.2059 (2)	7.4502 (2)	672.05 (6)	0.72999 (2)
500	10.2281 (3)	7.4751 (2)	677.24 (7)	0.73084 (3)
600	10.2497 (3)	7.5070 (3)	682.99 (8)	0.73241 (3)

[a] Number in the parentheses represents one standard deviation in the rightmost digit

insignificant deviation from ideal mixing for all unit-cell parameters, suggesting that the Vegard's law generally holds for this solid solution. Specifically, the deviation from the Vegard's law in the cases of the *a*-axis, *c*-axis, and volume is negative for the apatites with $x < 4$ and positive for the apatites with $x > 4$; this pattern, however, is reversed in the case of the *c*/*a* ratio. For the calcium phosphate and vanadate apatite solid solution in comparison ($Ca_{10}[(PO_4)_{6-x}(VO_4)_x](OH)_2$; Kim et al. 2000; Boechat et al. 2000), insignificant deviation from the Vegard's law is also observed for all the unit-cell parameters (Fig. 3).

Volume-composition relationship of a binary solid solution such as the one investigated here is usually regarded as a good indicator of the general thermodynamic properties of the solid solution. As pointed out by Kerrick and Darken (1975), the larger the difference is in the molar volumes between two end-members of a binary system, the greater the possibility is for them to deviate away from an ideal solid solution. For binary oxide systems and silicate systems which behave ideally, the maximum difference in the molar volumes is about 5% (Kerrick and Darken 1975). The maximum volume difference in the $Pb_{10}[(PO_4)_{6-x}(VO_4)_x]F_2$ binary solid solution is about 8% (Table 2), that of the $Ca_{10}[(PO_4)_{6-x}(VO_4)_x](OH)_2$ solid solution about 8% (Kim et al. 2000; Boechat et al. 2000), that of $Pb_{10}[(PO_4)_{6-x}(VO_4)_x]Cl_2$ about 6.5% (Chernorukov et al. 2010), and that of $Pb_{10}(PO_4)_6(F_{2-x}Cl_x)$ about 2.4% (Knyazev et al. 2011). All these solid solutions are non-ideal. The non-ideal solid solution behavior of the first three apatite solid solutions is understood by referring to the large difference of the volumes between the end-members, while that of the $Pb_{10}(PO_4)_6(F_{2-x}Cl_x)$ solid solution is probably related to the different positions of the F and Cl atoms in the *c*-axis channel of the apatites (Kim et al. 2000).

As previously mentioned, the synthetic apatites from Chernorukov et al. ($Pb_{10}[(PO_4)_{6-x}(VO_4)_x]Cl_2$; 2010) and Knyazev et al. ($Pb_{10}(PO_4)_6(F_{2-x}Cl_x)$; 2011) might be problematic, so that the solid solution behavior of the apatites established by these two studies should be treated with great caution. Due to the much lower experimental temperatures and much shorter synthesizing durations (at 350–700°C for about 10 h; Chernorukov et al. 2010; Knyazev et al. 2011), these apatites were too fine to be compositionally analyzed. Additionally, SEM was not employed to check for any potential trace phases. The open porcelain crucible used in the synthesizing experiments, however, might lead to the loss of Pb to porcelain and the loss of F and Cl to open air during sample-synthesizing at high temperatures (Hata et al. 1980), which eventually should result in some trace phases and variable apatite compositions. This possibility has been well hinted by the room-T volume of the assumed $Pb_{10}(PO_4)_6F_2$ apatite (621.3 Å^3; Knyazev et al. 2011), which is close to the volume of the $Pb_9(PO_4)_6$ apatite ($\sim$615 Å^3; Hata et al. 1980) rather than the well-established value of about 600 Å^3 for the $Pb_{10}(PO_4)_6F_2$ apatite (Merker and Wondratschek 1959; Kreidler and Hummel 1970; Grisafe and Hummel 1970; Kim et al. 2000; Liu et al. 2008; Fleet et al. 2010). On the other hand, the $Pb_{10}(PO_4)_6Cl_2$ apatite synthesized by Chernorukov et al. (2010) and Knyazev et al. (2011) appeared problem-free since its volume was very compatible with the literature data ($\sim$631 Å^3; Merker and Wondratschek 1959; Kreidler and Hummel 1970; Grisafe and Hummel 1970; Kim et al. 2000). Nevertheless, the uncertainty in the apatite compositions certainly impaired the proposed regular solution models for these two binary systems.

Raman feature

Both lead fluorapatite and lead fluorvanadate apatite have the crystal structure of $P6_3/m$, with six tetrahedral BO_4 units in the primitive unit cell $Pb_{10}[(PO_4)_{6-x}(VO_4)_x]F_2$. The vibrational spectrum of apatites is mainly about the BO_4 ions. For the free form of BO_4 ion (B = P or V, with symmetry of T_d), the symmetric stretching mode ν_1 is nondegenerate, asymmetric stretching mode ν_3 is triply degenerate, and the corresponding bending vibrations ν_2 and ν_4 are doubly degenerate and triply degenerate, respectively (Beran et al. 2004). In the crystal structure of the apatites, the distorted BO_4 ions with the site symmetry of C_s (Bhatnager 1971) should have 4 stretching bands and

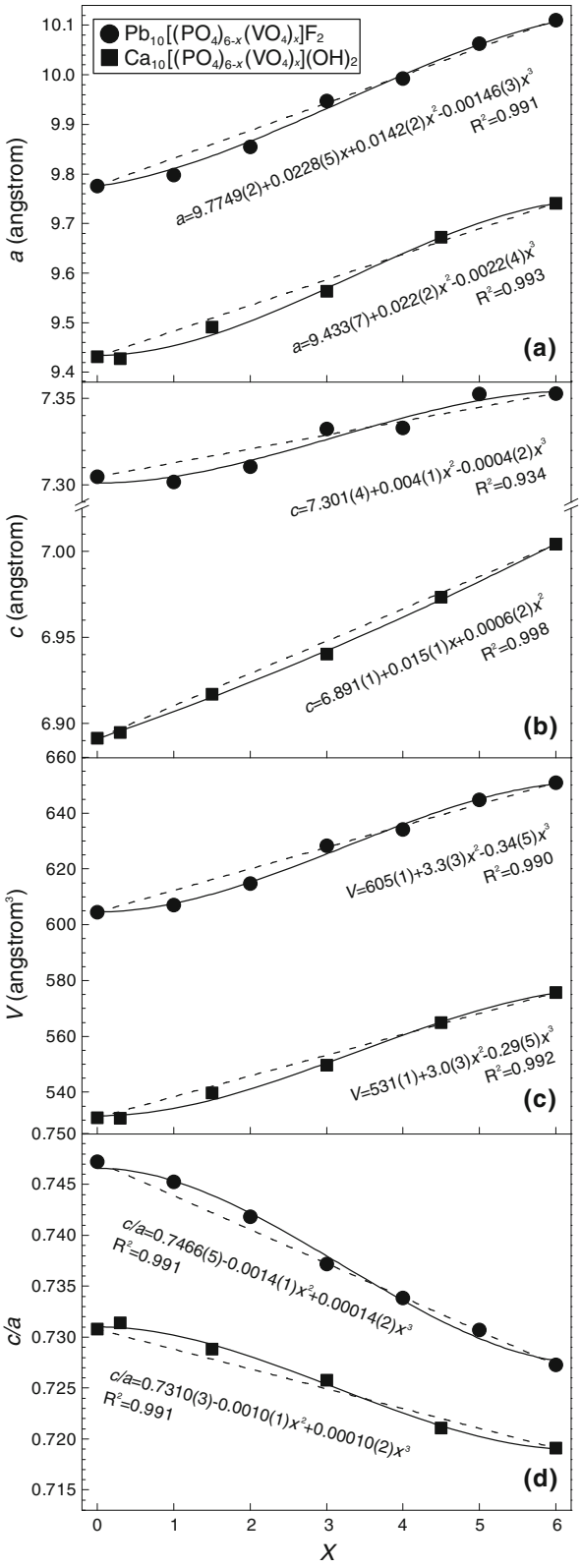

◀**Fig. 3** Effect of composition on the unit-cell parameters of the apatite solid solution $Pb_{10}[(PO_4)_{6-x}(VO_4)_x]F_2$ (*filled circles*; this study) and $Ca_{10}[(PO_4)_{6-x}(VO_4)_x](OH)_2$ (*filled squares*): **a** the *a*-axis; **b** the *c*-axis; **c** the volume; and **d** the *c*/*a* ratio. Data for the $Ca_{10}[(PO_4)_{6-x}(VO_4)_x](OH)_2$ solid solution are from Kim et al. (2000; $x = 0.0$) and Boechat et al. (2000; $x = 0.3$, 1.5, 3.0, 4.5 and 6.0). The composition of the apatites from Kim et al. (2000) was not quantified, whereas those from Boechat et al. (2000) were constrained by inductively coupled plasma

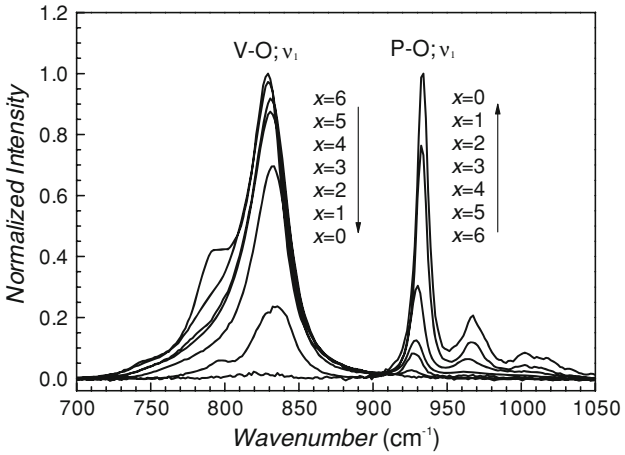

Fig. 4 Raman spectra of the apatite solid solution $Pb_{10}[(PO_4)_{6-x}(VO_4)_x]F_2$. In order to remove the difference in the analytical condition among different analyses, the sum of the intensities of the symmetric stretching vibration of the PO_4^{3-} and VO_4^{3-} ions was defined as 1, and subsequently the spectrum was normalized to it

5 bending bands ($1\nu_1 + 3\nu_3 + 2\nu_2 + 3\nu_4 = 9$), which are all Raman-active. If strong interaction among the BO_4 ions and coupling of their vibrational modes present, these bands should further split into 15 internal vibrational modes ($6A_g$, $3E_{1g}$, and $6E_{2g}$), as predicted by the factor-group analysis (Klee 1970; Levitt and Condrate 1970), which include $2\nu_1$ ($A_g + E_{2g}$), $5\nu_3$ ($2A_g + E_{1g} + 2E_{2g}$), $3\nu_2$ ($A_{1g} + E_{1g} + E_{2g}$), and $5\nu_4$ ($2A_g + 2E_{2g} + E_{1g}$).

The Raman spectra of the solid solution of lead fluorapatite and lead fluorvanadate apatite are shown in Fig. 4. The bands from 900 to 1,050 cm^{-1} are assigned to the ν_1 symmetric stretching vibration and ν_3 asymmetric stretching vibration of the phosphate ion, while those from 700 to 900 cm^{-1} are assigned to the vanadate ion (Adler 1964, 1968; Levitt and Condrate 1970; Bhatnager 1971). As the composition changes, both the spectrum shape and band position vary systematically.

The band-component analyses of the Raman spectra of the phosphate and vanadate ions are shown in Fig. 5, with the former best illustrated using the V-free sample (HL019) and the latter using the P-free sample (HL010). In the 900–1,050 cm^{-1} region (Fig. 5a), four bands are generally detected for the phosphate ion at 933.4, 967.9, 1,002.6, and 1,017.4 cm^{-1}. In accordance with the literature data (Table 3), the first band is attributed to the symmetric stretching vibration of the PO_4^{3-} ion, while the left three bands are attributed to the asymmetric stretching vibration.

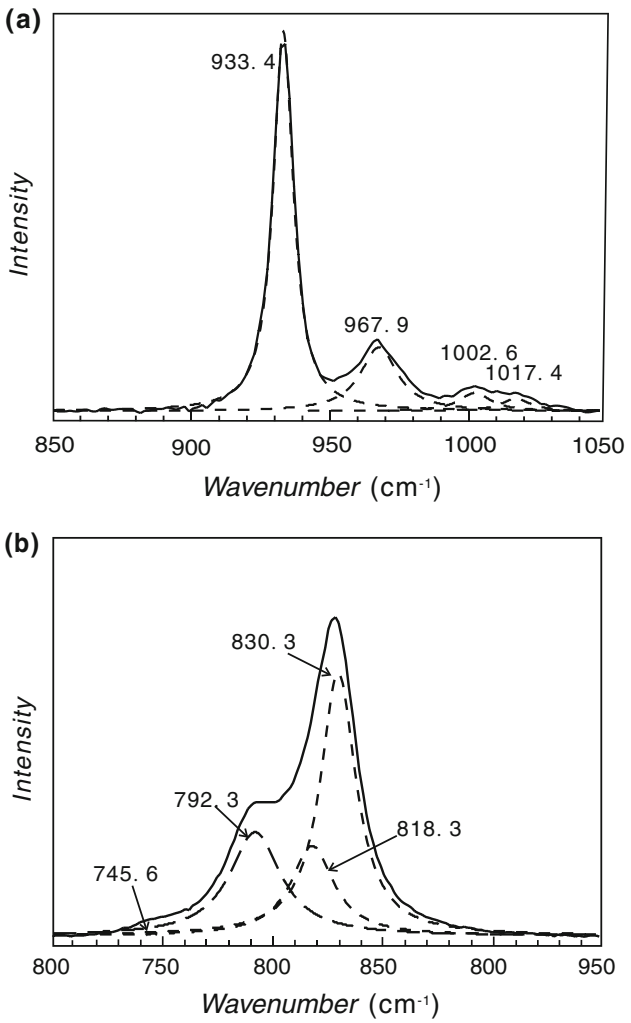

Fig. 5 Raman spectroscopic analysis for PO_4^{3-} (**a**) and VO_4^{3-} (**b**) in the stretching region. Spectrum shown in (**a**) was taken on HL019 whereas that in (**b**) was taken on HL010 (Table 1)

In the 700–900 cm^{-1} region (Fig. 5b), two bands are clearly observed for the vanadate ion at 830.3 and 792.3 cm^{-1}. Since the Raman band at 830.3 cm^{-1} is asymmetric, another band at 818.3 cm^{-1} may be resolved. In addition, there is a very weak band at 745.6 cm^{-1} which highly possibly belongs to the vanadate ion. According to the literature data (Adler 1968; Levitt and Condrate 1970; Bhatnager 1971; Frost et al. 2003; Eon et al. 2006; Zhang et al. 2007), we assign the band at 830.3 cm^{-1} to the symmetric stretching vibration and other bands to the asymmetric stretching vibration of the vanadate ion (Table 3). Since both ions have $1v_1$ band and $3v_3$ bands, their symmetric states are thus similar and both P and V are on a C_s site, indicating negligible factor-group effect (Levitt and Condrate 1970; Bhatnager 1971). In contrast, Frost and Palmer (2007) deconvoluted their spectra into more components and claimed a reduced symmetry for the PO_4^{3-} ions in the pyromorphite $Pb_{10}(PO_4)_6Cl_2$.

The Raman frequencies of the PO_4^{3-} and VO_4^{3-} symmetric stretching mode v_1 of the solid solution between lead fluorapatite and lead fluorvanadate apatite (Table 4) are shown in Fig. 6. Apparently, the frequencies are almost linearly correlated with the composition and gradually shift to lower wavenumbers as the content of V increases. It follows that the P and V cations in the BO_4 tetrahedra must gradually change their sizes as their proportions vary (Hardcastle and Wachs 1991; Popović et al. 2005). This phenomenon is fully compatible with early observations made with the PO_4^{-} substituted vanadinite (Adler 1964) and the calcium phosphate and vanadate hydroxyapatite solid solution (Boechat et al. 2000). Since the BO_4 tetrahedron is the most incompressible structural unit in the apatite structure (Comodi et al. 2001), its large influence on the sizes of P and V seems reasonable.

Additionally, the Raman data from this investigation have demonstrated that the frequencies of the PO_4^{3-} and VO_4^{3-} symmetric stretching mode v_1 of the solid solution between lead fluorapatite and lead fluorvanadate apatite well correlate with the PO_4^{3-} and VO_4^{3-} contents. The established equations, shown in Fig. 6, apparently provide an inexpensive and convenient analytical method for the contents of these components in lead apatites.

Thermal expansivity

The high-*T* X-ray data suggest that the lead fluorapatite and lead fluorvanadate apatite solid solution is stable (or metastable due to potential kinetic reasons) up to at least 600°C. At 700°C, these apatites start to be unstable, which seems surprising since they were synthesized at 700°C and 1 atm. The major difference between the synthesizing experiments and high-*T* X-ray diffraction experiments is that the former was conducted in closed system, whereas the latter was carried out in open air. As suggested by Hata et al. (1980), synthesizing apatites in open air at high temperatures might lead to different and volatile-free product (for example, $Pb_9(PO_4)_6$).

The room-*P* unit-cell parameters at temperatures up to 600°C (Table 2) are shown in Fig. 7. Apparently, these unit-cell parameters are generally in a good linear relation with *T*, indicating that the thermal expansion coefficients are *T*-independent in the investigated temperature range. Consequently, we fitted the room-*P* unit-cell parameters at different temperatures with the equation $j = j_0 e^{\alpha_j(T-T_0)}$ to derive the thermal expansion coefficients $\alpha_j = j^{-1}(\partial j/\partial T)$, where *j* stands for *a*, *c,* or *V*. The derived thermal expansion coefficients are listed in Table 5 and shown in Fig. 8. Evidently, the thermal expansion coefficients generally vary linearly with the composition, and the maximum amount of variation in the volumetric thermal expansion

Table 3 Band-component analysis of the Raman spectrum of the PO_4^{3-} and VO_4^{3-} cations in apatite solid solution $Pb_{10}[(PO_4)_{6-x}(VO_4)_x]F_2$ (stretching vibration)

I/R[a]	Symmetric	Asymmetric			Chemical formula	Data source
	v_1	v_3				
PO_4^{3-}						
I	922	967	–	1026	$Pb_{10}(PO_4)_6Cl_2$	Adler (1968)
I	925	968	–	1028	$Pb_{10}(PO_4)_6Cl_2$	Bhatnager (1971)
I	927	967	999	1031	$Pb_{10}(PO_4)_6Cl_2$	Levitt and Condrate (1970)
R	920	947	980	1014	$Pb_{10}(PO_4)_6Cl_2$	Levitt and Condrate (1970)
I	919	953	974	1020	$Pb_{10}(PO_4)_6Cl_2$	Bartholomäi and Klee (1978)
R	920	949	981 (?)	1025	$Pb_{10}(PO_4)_6Cl_2$	Bartholomäi and Klee (1978)
I	916	952	1009	–	$Pb_{10}(PO_4)_6Cl_2$	Frost and Palmer (2007)[b]
R	923	946	980	1027	$Pb_{10}(PO_4)_6Cl_2$	Frost and Palmer (2007)[b]
I	922	961	–	1026	$Pb_{10}(PO_4)_6Cl_2$	Chernorukov et al. (2010)
I	922	959	982	1031	$Pb_{10}(PO_4)_6Cl_2$	Knyazev et al. (2011)
I	922	961	–	1026	$Pb_{10}(PO_4)_6F_2$	Knyazev et al. (2011)
R	933	968	1003	1017	$Pb_{10}(PO_4)_6F_2$	This study
VO_4^{3-}						
I	–	–	800	736	$Pb_{10}(VO_4)_6Cl_2$	Adler (1968)
I	–	–	805	740	$Pb_{10}(VO_4)_6Cl_2$	Bhatnager (1971)
I	–	830	801	737	$Pb_{10}(VO_4)_6Cl_2$	Levitt and Condrate (1970)
R	825	–	793	722	$Pb_{10}(VO_4)_6Cl_2$	Levitt and Condrate (1970)
I	828	790	762	719	$Pb_{10}(VO_4)_6Cl_2$	Bartholomäi and Klee (1978)
R	826	798	770 (?)	721	$Pb_{10}(VO_4)_6Cl_2$	Bartholomäi and Klee (1978)
R	827	815	790	730	$Pb_{10}(VO_4)_6Cl_2$	Frost et al. (2003)
R	825	817	788	737	$Pb_{10}(VO_4)_6(OH)_2$	Eon et al. (2006)
I	862	834	779	724	$Pb_{10}(VO_4)_6I_2$	Zhang et al. (2007)[c]
I	–	810	–	739	$Pb_{10}(VO_4)_6Cl_2$	Chernorukov et al. (2010)
R	830	818	792	746	$Pb_{10}(VO_4)_6F_2$	This study

[a] *I* infrared, *R* Raman

[b] Sample #: Pyromorphite 3

[c] Untreated sample

Table 4 Symmetric stretching vibration of the PO_4^{3-} and VO_4^{3-} cations in apatite solid solution $Pb_{10}[(PO_4)_{6-x}(VO_4)_x]F_2$

Sample #	x	VO_4 (v_1)		PO_4 (v_1)	
		Frequency (cm^{-1})	Intensity[a]	Frequency (cm^{-1})	Intensity
HL019	0	–	–	933.4 (1)[b]	1.00 (1)
HL020	1	834.1 (3)	0.20 (2)	932.7 (1)	0.80 (1)
HL021	2	832.9 (2)	0.58 (9)	929.8 (1)	0.42 (3)
HL016	3	832.7 (3)	0.83 (17)	928.9 (1)	0.17 (2)
HL017	4	832.2 (2)	0.89 (14)	928.2 (2)	0.11 (1)
HL018	5	830.9 (1)	0.97 (5)	926.7 (4)	0.03 (1)
HL010	6	830.0 (2)	1.00 (11)	–	–

[a] Intensity is normalized to the sum of the intensities of the v_1 bands of the PO_4^{3-} and VO_4^{3-} cations

[b] Number in the parentheses represents one standard deviation in the rightmost digit

coefficients is about 13% (from $7.30(15) \times 10^{-5}$/°C for $Pb_{10}(PO_4)_6F_2$ to $8.28(22) \times 10^{-5}$/°C for $Pb_{10}(VO_4)_6F_2$). The increase in the thermal expansivity caused by the substitution of the VO_4 tetrahedra for the PO_4 tetrahedra should be expected since the V–O bonds are longer and weaker than the P–O bonds.

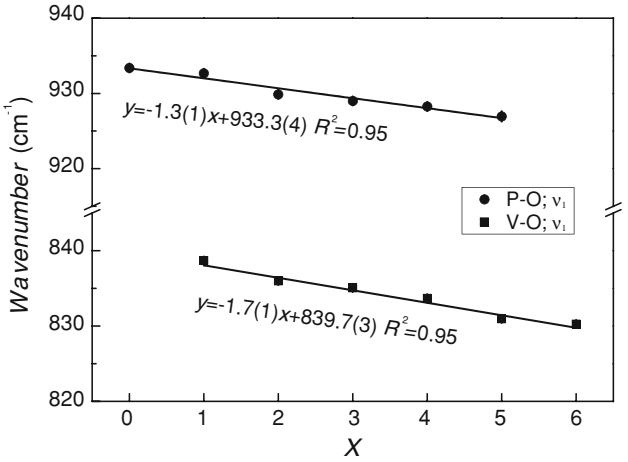

Fig. 6 Effect of composition on the symmetric stretching vibration of the PO_4^{3-} and VO_4^{3-} ions

The thermal expansivity of various calcium apatites has been experimentally investigated at room pressure, and the unit-cell parameters are generally in good linear relationship with temperature at least up to 600°C (Fischer et al. 1983; Bauer and Klee 1993; Brunet et al. 1999; Tonegawa et al. 2010). For the purpose of comparison, we have reprocessed the *V*-*T* data ($T \leq 600$°C) in the literature and obtained $\alpha_V = 4.5(5) \times 10^{-5}$/°C for $Ca_{10}(PO_4)_6(OH)_2$ (Fischer et al. 1983), $\alpha_V = 3.9(2) \times 10^{-5}$/°C for $Ca_{10}(PO_4)_6(OH)_2$ (Brunet et al. 1999), $\alpha_V = 4.3(1) \times 10^{-5}$/°C for $Ca_{10}(PO_4)_6F_2$ (Brunet et al. 1999), $\alpha_V = 3.56(1) \times 10^{-5}$/°C for $Ca_{10}(PO_4)_6Cl_2$ (Brunet et al. 1999), and $\alpha_V = 4.0(2) \times 10^{-5}$/°C for type A carbonate apatite ($Ca_{10}(PO_4)_6(CO_3)$; Tonegawa et al. 2010).

Recently, the thermal expansivity of some lead apatites was experimentally investigated by Chernorukov et al. (2010) and Knyazev et al. (2011), which did not disclose any details about their high-*T* X-ray diffraction experiments. We also reprocessed their *V*-*T* data ($T \leq 600$°C) and obtained $\alpha_V = 5.2(1) \times 10^{-5}$/°C for $Pb_{10}(VO_4)_6Cl_2$ (Chernorukov et al. 2010), $\alpha_V = 4.9(1) \times 10^{-5}$/°C for $Pb_{10}(PO_4)_6Cl_2$ (Knyazev et al. 2011), and $\alpha_V = 4.7(2) \times 10^{-5}$/°C for $Pb_{10}(PO_4)_6F_2$ (Knyazev et al. 2011). Apparently, the thermal expansivity of $Pb_{10}(PO_4)_6F_2$ obtained by Knyazev et al. (2011) is much different to our result ($\alpha_V = 7.30(15) \times 10^{-5}$/°C; Table 5). For the $Pb_{10}[(PO_4)_{6-x}(VO_4)_x]Cl_2$ solid solution, the variation in the thermal expansivity is about 6%, which is only about half of that of the $Pb_{10}[(PO_4)_{6-x}(VO_4)_x]F_2$ solid solution. It has to point out here that the results from Chernorukov et al. (2010) and Knyazev et al. (2011), however, must be viewed with great caution, considering the potential problems in their synthetic samples as mentioned earlier.

For the calcium apatites, the maximum amount of variation in the thermal expansivity caused by the

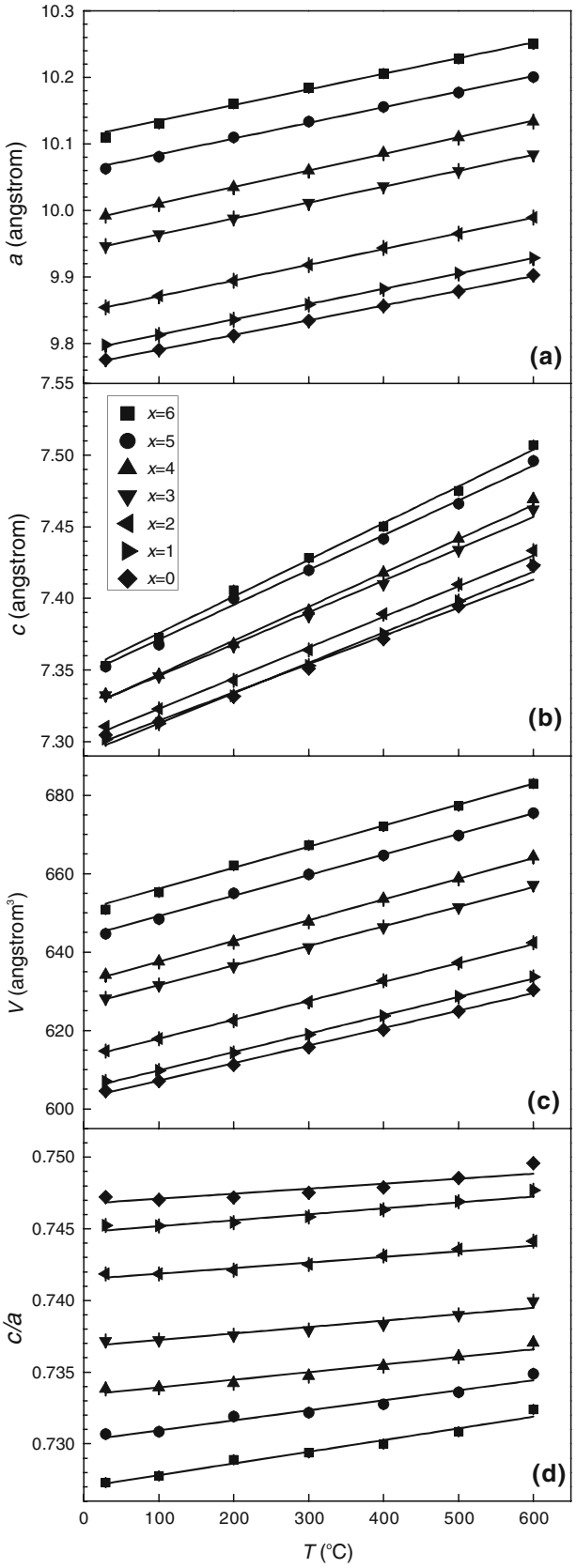

Fig. 7 Evolution of unit-cell parameters *a*, *c*, *V*, and *c*/*a* of the apatite solid solution $Pb_{10}[(PO_4)_{6-x}(VO_4)_x]F_2$ with temperature

Table 5 Thermal expansion coefficients of apatite solid solution $Pb_{10}[(PO_4)_{6-x}(VO_4)_x]F_2$

x	α_a (10^{-5})[a]	α_c (10^{-5})	α_V (10^{-5})
0	2.25 (2)[b]	2.79 (12)	7.30 (15)
1	2.33 (1)	2.91 (7)	7.57 (8)
2	2.38 (2)	2.95 (5)	7.72 (7)
3	2.40 (1)	3.04 (7)	7.83 (8)
4	2.47 (2)	3.24 (7)	8.19 (7)
5	2.37 (6)	3.33 (8)	8.07 (17)
6	2.38 (7)	3.53 (10)	8.28 (22)

[a] Thermal expansion coefficients are in $°C^{-1}$

[b] Number in the parentheses represents one standard deviation in the rightmost digit

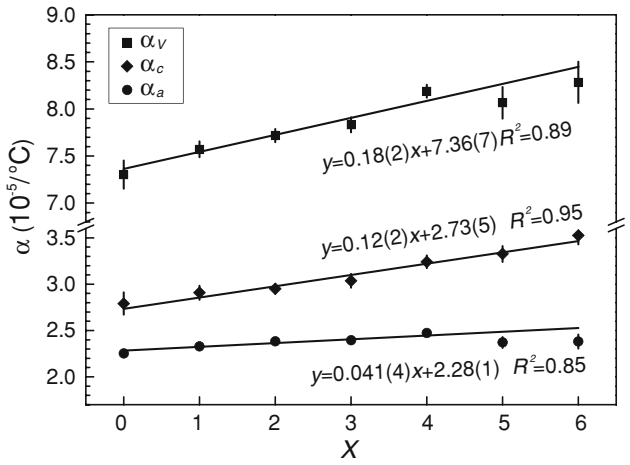

Fig. 8 Effect of composition on the thermal expansion coefficient of the apatite solid solution $Pb_{10}[(PO_4)_{6-x}(VO_4)_x]F_2$

compositional difference on the X site is about 26% (from 3.56(1) × 10^{-5}/°C for $Ca_{10}(PO_4)_6Cl_2$ to 4.5(5) × 10^{-5}/°C for $Ca_{10}(PO_4)_6(OH)_2$). For the lead apatites, the maximum amount of variation in the thermal expansivity caused by the compositional difference on the X site is much less, about 4% (from 4.9(1) × 10^{-5}/°C for $Pb_{10}(PO_4)_6Cl_2$ to 4.7(2) × 10^{-5}/°C for $Pb_{10}(PO_4)_6F_2$), according to the *V-T* data from Knyazev et al. (2011). It appears that the effect of the X-site compositional difference on the thermal expansivity of apatites is very variable, and much affected by the ion species on the M site.

As to the effect of the B-site compositional difference on the thermal expansivity, this study suggested a value of about 13% for the $Pb_{10}[(PO_4)_{6-x}(VO_4)_x]F_2$ solid solution, and the data from Chernorukov et al. (2010) and Knyazev et al. (2011) suggested a value of about 6% for the $Pb_{10}[(PO_4)_{6-x}(VO_4)_x]Cl_2$ solid solution. Thus, the effect of the B-site compositional difference on the thermal expansivity is also variable and affected by the X species.

As to the effect of the M-site compositional difference on the thermal expansivity, the existing investigations suggested values of about 38% for the $(Ca_{10-x}Pb_x)(PO_4)_6Cl_2$ solid solution (Brunet et al. 1999; Chernorukov et al. 2010) and 70% for the $(Ca_{10-x}Pb_x)(PO_4)_6F_2$ solid solution (Brunet et al. 1999; This study). If the data of the problematic $Pb_{10}(PO_4)_6F_2$ apatite from Knyazev et al. (2011; 4.7(2) × 10^{-5}/°C) is used, the effect of the M-site compositional difference on the thermal expansivity of the $(Ca_{10-x}Pb_x)(PO_4)_6F_2$ solid solution decreases to just about 9%, which is unusually low. Anyhow, it is reasonable to conclude that the effect of the M-site compositional difference on the thermal expansivity is not only variable, but also affected by the X species.

Summarily, the influence of the X-site and B-site compositional difference on the thermal expansivity of apatites is generally small, while that of the M-site compositional difference is large. This argument is in good agreement with the crystallographic features of apatites (Sha et al. 1994; Comodi et al. 2001) and available compression data at ambient temperature (Brunet et al. 1999; Matsukage et al. 2004; Liu et al. 2008, 2011a, c; Fleet et al. 2010).

Acknowledgments We are grateful to two anonymous reviewers and Professor M. Matsui who provided critical comments on the manuscript. We thank the National Natural Science Foundation of China (Grant 40872033) for financial support.

References

Adler HH (1964) Infrared spectra of phosphate minerals: symmetry and substitutional effects in the pyromorphite series. Am Mineral 49:1002–1015

Adler HH (1968) Infrared spectra of phosphate minerals: splitting and frequency shifts associated with substitution of PO_4^{3-} for AsO_4^{3-} in mimetite ($Pb_5(AsO_4)_3Cl$). Am Mineral 53:1740–1744

Badraoui B, Aissa A, Bigi A, Debbabi M, Gazzano M (2006) Structural investigations of lead-strontium fluoroapatites. J Solid State Chem 179:3065–3072

Baker WE (1966) An X-ray diffraction study of synthetic members of the pyromorphite series. Am Mineral 51:1712–1721

Bartholomäi G, Klee WE (1978) The vibrational spectra of pyromorphite, vanadinite and mimetite. Spectrochim Acta 34A: 831–843

Bauer M, Klee WE (1993) The monoclinic-hexagonal phase transition in chlorapatite. Eur J Mineral 5:307–316

Belokoneva EL, Troneva EA, Dem'yanets LN, Duderov NG, Belov NV (1982) Crystal structure of synthetic fluoropyromorphite $Pb_5(PO_4)_3F$. Sov Phys Crystallogr 27:476–477

Beran A, Voll D, Schneider H (2004) IR spectroscopy as a tool for the characterization of ceramic precursor phases. In: Beran A, Libowitzky E (eds) Spectroscopic methods in mineralogy. EMU notes in mineralogy, vol 6. European Mineralogical Union, Budapest, pp 189–226

Bhatnager VM (1971) X-ray and Infrared studies of lead apatites. Can J Chem 49:662–663

Boechat CB, Eon J-G, Rossi AM, Andre′ de Castro Perez C, Aguiar da Silva San Gil R (2000) Structure of vanadate in calcium phosphate and vanadate apatite solid solutions. Phys Chem Chem Phys 2:4225–4230

Brunet F, Allan DR, Redfern SAT, Angel RJ, Miletich RM, Reichmann HJ, Sergent J, Hanfland M (1999) Compressibility and thermal expansivity of synthetic apatites, $Ca_5(PO_4)_3X$ with X = OH, F and Cl. Eur J Mineral 11:1023–1035

Chernorukov NG, Knyazev AV, Bulanov EN (2010) Isomorphism and phase diagram of the $Pb_5(PO_4)_3Cl$-$Pb_5(VO_4)_3Cl$ system. Russ J Inorg Chem 55:1463–1470

Cockbain AG (1968) Lead apatite solid-solution series. Mineral Mag 36:1171–1173

Comodi P, Liu Y, Zanazzi PF, Montagnoli M (2001) Structural and vibrational behaviour of fluorapatite with pressure. Part I: in situ single-crystal X-ray diffraction investigation. Phys Chem Mineral 28:219–224

Dong ZL, White TJ, Sun K, Wang LM, Ewing RC (2005) Electron irradiation induced transformation of $(Pb_5Ca_5)(VO_4)_6F_2$ apatite to $CaVO_3$ perovskite. J Am Ceram Soc 88:184–190

Elliott JC (2002) Calcium phosphates biominerals. In: Kohn MJ, Rakovan J, Hughes JM (eds) Phosphates. Reviews in mineralogy and geochemistry, vol 48. Mineralogical Society of America, Chantilly, pp 427–453

Eon JG, Boechat CB, Rossi AM, Terra J, Ellis DE (2006) A structural analysis of lead hydroxyvanadinite. Phys Chem Chem Phys 8:1845–1851

Fischer GR, Bardhan P, Geiger JE (1983) The lattice thermal expansion of hydroxyapatite. J Mater Sci Lett 2:577–578

Fleet ME, Liu X, Shieh SR (2010) Structural change in lead fluorapatite at high pressure. Phys Chem Mineral 37:1–9

Frost RL, Palmer SJ (2007) A Raman spectroscopic study of the phosphate mineral pyromorphite $Pb_5(PO_4)_3Cl$. Polyhedron 26:4533–4541

Frost RL, Crane M, Williams PA, Theo Kloprogge J (2003) Isomorphic substitution in vanadinite $[Pb_5(VO_4)_3Cl]$-a Raman spectroscopic study. J Raman Spectrosc 34:214–220

Grisafe DA, Hummel FA (1970) Pentavalent Ion substitution in the apatite structure part A. Crystal chemistry. J Solid State Chem 2:160–166

Gupta SK, Rao PVR, Narasaraju TSB (1986) Physico-chemical aspects of calcium vanadate apatite. J Mater Sci 21:161–164

Hardcastle FD, Wachs IE (1991) Determination of vanadium-oxygen bond distances and bond orders by Raman spectroscopy. J Phys Chem 95:5031–5041

Hata M, Marumo F, Iwai SI (1980) Structure of a lead apatite $Pb_9(PO_4)_6$. Acta Cryst B36:2128–2130

Hu X, Liu X, He Q, Wang H, Qin S, Ren L, Wu C, Chang L (2011) Thermal expansion of andalusite and sillimanite at ambient pressure: a powder X-ray diffraction study up to 1,000°C. Mineral Mag 75:363–374

Hughes JM, Rakovan J (2002) The crystal structure of apatite, Ca5(PO4)3(F, OH, Cl). In: Kohn MJ, Rakovan J, Hughes JM (eds) Phosphates. Reviews in Mineralogy and Geochemistry, vol 48. Mineralogical Society of America, Chantilly, pp 1–12

Kerrick DM, Darken LS (1975) Statistical thermodynamic models for ideal oxide and silicate solid solutions, with application to plagioclase. Geochim Cosmochim Acta 39:1431–1442

Kim JY, Fenton RR, Hunter BA, Kennedy BJ (2000) Powder diffraction studies of synthetic calcium and lead apatites. Aust J Chem 53:679–686

Kim JY, Dong Z, White TJ (2005) Model apatite systems for the stabilization of toxic metals: II, Cation and metalloid substitutions in chlorapatites. J Am Ceram Soc 88:1253–1260

Klee WE (1970) The vibrational spectra of the phosphate ions in fluorapatite. Zeit Kristallogr 131:95–102

Knyazev AV, Chernorukov NG, Bulanov EN (2011) Isomorphism and phase diagram of $Pb_5(PO_4)_3F$-$Pb_5(PO_4)_3Cl$ system. Thermochim Acta 513:112–118

Kreidler ER, Hummel FA (1970) The crystal chemistry of apatite: structure fields of fluor- and chlorapatite. Am Mineral 55:170–184

Lang JR, Lueck B, Mortensen JK, Kelly Russell J, Stanley CR, Thompson JFH (1995) Triassic-Jurassic silica-undersaturated and silica-saturated alkalic intrusions in the Cordillera of British Columbia: implications for arc magmatism. Geology 23: 451–454

Levitt SR, Condrate RA (1970) The vibrational spectra of lead apatites. Am Mineral 55:1562–1575

Liu X, Shieh SR, Fleet ME, Akhmetov A (2008) High-pressure study on lead fluorapatite. Am Mineral 93:1581–1584

Liu X, He Q, Wang H, Fleet ME, Hu X (2010) Thermal expansion of kyanite at ambient pressure: an X-ray powder diffraction study up to 1000°C. Geosci Front 1:91–97

Liu X, Fleet ME, Shieh SR, He Q (2011a) Synthetic lead bromapatite: x-ray structure at ambient pressure and compressibility up to about 20 GPa. Phys Chem Mineral 38:397–406

Liu X, Liu W, He Q, Deng L, Wang H, He D, Li B (2011b) Isotropic thermal expansivity and anisotropic compressibility of ReB_2. Chin Phys Lett 28:036401

Liu X, Shieh SR, Fleet ME, Zhang L, He Q (2011c) Equation of state of carbonated hydroxylapatite at ambient temperature: significance of carbonate. Am Mineral 96:74–80

Ma QY, Traina SJ, Logan TJ, Ryan JA (1993) In situ lead immobilization by apatite. Environ Sci Technol 27:1803–1810

Matsukage KN, Ono S, Kawamoto T, Kikegawa T (2004) The compressibility of a natural apatite. Phys Chem Mineral 31: 580–584

Mercier PHJ, Dong Z, Baikie T, Le Page Y, White TJ, Whitfield PS, Mitchel LD (2007) Ab initio constrained crystal-chemical Rietveld refinement of $Ca_{10}(V_xP_{1-x}O_4)_6F_2$ apatites. Acta Cryst B63:37–48

Merker L, Wondratschek H (1959) Bleiverbindungen mit Apatitstruktur, insbesondere Blei-Jod-und Blei-Brom-Apatite. Z Anorg Allg Chem 300:41–50

Miyake M, Ishigaki K, Suzuki T (1986) Structure refinements of Pb^{2+} ion-exchanged apatites by X-ray powder pattern-fitting. J Solid State Chem 61:230–235

Pan Y, Fleet ME (2002) Compositions of the apatite-group minerals: substitution mechanisms and controlling factors. In: Kohn MJ, Rakovan J, Hughes JM (eds) Phosphates. Reviews in mineralogy and geochemistry, vol 48. Mineralogical Society of America, Chantilly, pp 13–49

Podsiadlo H (1990) Polymorphic transitions in the binary system lead fluorapatite [Pb10(PO4)6Cl2]–calcium fluorapatite [Ca10(PO4) 6Cl2]. J Therm Anal 36:569–575

Popović L, de Waal D, Boeyens JCA (2005) Correlation between Raman wavenumbers and P-O bond lengths in crystalline inorganic phosphates. J Raman Spectrosc 36:2–11

Ruszala F, Kostiner E (1975) Preparation and characterization of single crystals in the apatite system Ca10(PO4)6(Cl, OH)2. J Crystal Growth 30:93–95

Sha MC, Li Z, Brad RC (1994) Single-crystal elastic constants of fluorapatite, $Ca_5F(PO_4)_3$. J Appl Phys 75:7784–7787

Suzuki T, Ishigaki K, Miyake M (1984) Synthetic hydroxyapatites as inorganic cation exchangers. J Chem Soc Faraday Trans I 80:3157–3165

Tonegawa T, Ikoma T, Suetsugu Y, Igawa N, Matsushita Y, Yoshioka T, Hanagata N, Tanaka J (2010) Thermal expansion of type A carbonate apatite. Mater Sci Eng B 173:171–175

Zhang M, Maddrell ER, Abraitis PK, Salje EKH (2007) Impact of leach on lead vanado-iodoapatite $[Pb_5(VO_4)_3I]$: an infrared and Raman spectroscopic study. Mater Sci Eng B 137:149–155